ACS Catalysis

LETTER

pubs.acs.org/acscatalysis

SnO_x—$ZnGa_2O_4$ Photocatalysts with Enhanced Visible Light Activity

Venkata Bharat Ram Boppana and Raul F. Lobo*

Center for Catalytic Science and Technology, Department of Chemical Engineering, University of Delaware, Newark, Delaware 19716, United States

Supporting Information

ABSTRACT: Surface modification of zinc gallate with SnO_x species produces photocatalysts active for cresol oxidation using visible light. In these composite materials, the production rate of hydroxyl radicals and the cresol degradation rate just in visible light are higher than those with zinc gallate in UV light. The visible light absorbance in the newly introduced SnO_x surface phase is attributed to the presence of Sn^{2+} as confirmed using Mössbauer spectroscopy. Because cresol degradation proceeds via direct oxidation by holes, the increased degradation rates in UV and visible light suggest an increase in the effective photo-oxidative reactivity of holes produced in the photocatalyst system.

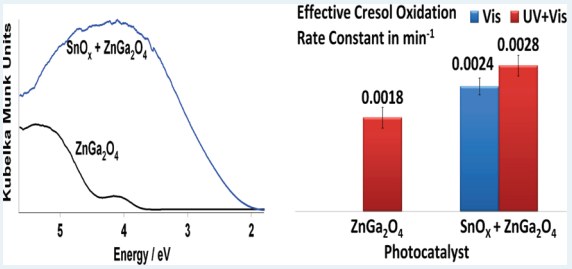

KEYWORDS: photocatalyst, photocatalysis, Sn 5s, visible light, SnO_x, $ZnGa_2O_4$

Development of visible-light-active photocatalysts is a significant challenge we need to overcome to harvest solar energy effectively.[1] The application of d^0 metal oxides such as TiO_2 for photocatalysis has been investigated extensively, yet this material has a wide band gap (>3 eV), making it ineffective for applications requiring photons in the visible range.[2,3] A number of research groups have investigated d^{10}-based photocatalysts, with noteworthy breakthroughs achieved for water splitting.[4−6] Zn^{2+} and Ga^{3+} are two d^{10} cations that in wurzite oxynitrides show the highest efficiencies for water splitting to date in visible light.[4] We have reported the incorporation of the same elements Zn−Ga−O−N in a spinel crystal with improved activity for methylene blue dye degradation compared with TiO_2 P25.[7,8] Still, these oxynitride catalysts are synthesized in an ammonia atmosphere at temperatures exceeding 550 °C with a concomitant formation of detrimental defects,[9] low surface areas, and oxygen vacancies (in the case of spinel Zn−Ga−O−N phase).[8] Other compounds such as $BiVO_4$,[10,11] $CaBi_2O_4$,[12] and Sn(II) niobates and tantalates[13] show considerable visible light activity, which is attributable to the presence of either Bi^{3+} 6s or Sn^{2+} 5s orbitals in their valence bands. The introduction of s character in the band structures hybridizes with O 2p orbitals, raising the maximum of the valence band and thereby reducing the band gap.[10] In this report, we show that a *surface* modification of a d^{10} semiconductor oxide with SnO_x surface species leads to visible light absorbance from the presence of Sn^{2+} (5s) orbitals and to an increase in the effective photo-oxidation reactivity of holes.[14]

Surface modification of a photocatalyst is a different approach from doping that circumvents the traditional drawbacks of doped semiconductors, that is, the generation of midgap or vacancy states.[15,16] For instance, a TiO_2 surface modified with Fe_2O_3 nanoparticles has shown visible absorbance and activity attributable to the presence of iron oxide particles on the surface and also due to improved charge separation.[15] Moreover, this Fe_2O_3 surface modification increases the activity in UV light, unlike traditional Fe-doped titania in which the introduced Fe^{2+} or Fe^{3+} dopant states can act as electron traps.[15−17] The improvements observed for Fe_2O_3—TiO_2 systems could also be explained as the result of surface oxide species that play the role of cocatalysts, thereby improving charge separation.[15,16] Here, we have applied this principle to hydrothermally synthesized $ZnGa_2O_4$, a d^{10} mixed-metal oxide photocatalyst with a wide band gap of 4.5 eV.[8,18] We have chosen SnO_x as the surface species because tin is inexpensive, nontoxic, and abundant, and prior reports have shown the formation of *yellow* tin oxide species (having the diffraction signatures of rutile SnO_2) when synthesized from $SnCl_2$.[19] Specifically, Firooz et al.[20] have observed the formation of yellow particles when synthesizing rutile SnO_2 from $SnCl_2$, as also observed in this report, although they have not verified for the presence of Sn^{2+}. On the other hand, when rutile SnO_2 is synthesized from $SnCl_4$, the product is *white*, with a wide band gap of 3.8 eV.[21,22]

Cation-doped oxides traditionally exhibit lower UV photocatalytic activity than their undoped precursors because the visible light transitions are affected by localized dopant midgap states, states that also act as electron traps.[17,23] Photocatalysts synthesized with photoactive surface species are rare and different because the enhanced activity is from the presence of a new surface metal oxide species (in this case, SnO_x), which improves charge separation, as seen previously with Fe_2O_3-[15,16] or FeOOH[24]-modified TiO_2. In this communication, we describe the synthesis of these photocatalysts and their characterization using X-ray diffraction (XRD), UV−vis diffuse reflectance

Received: March 11, 2011
Revised: June 18, 2011
Published: June 28, 2011

Table 1. Physical Properties of the $SnO_x - ZnGa_2O_4$ Materials

sample	tin source and concentration, mmol/L 0.1 N HCl	(311) fwhm, deg, 2θ	(311) coherence length, nm	band gap, eV	surface area, $m^2\ g^{-1}$	expected[a] Sn/(Sn + Zn + Ga)	measured bulk Sn/(Sn + Zn + Ga)[b]	measured surface Sn/(Sn + Zn + Ga)[c]
$ZnGa_2O_4$		0.48	22	4.5	55	0	0	0
SnZGO1	$SnCl_2$, 80	0.53	19.4	2.8	82	0.59	0.57	0.71
SnZGO2	$SnCl_2$, 160	0.54	19.0	2.8	62	0.74	0.69	0.81
SnZGO3	$SnCl_4$, 80	0.57	17.8	3.95	131	0.59		

[a] Metal molar ratio in the synthesis solution. [b] From SEM-EDAX measurements at low magnifications. [c] From XPS measurements, the band gap of SnO_x nanoparticles is 2.7 eV.

spectroscopy, scanning electron microscopy (SEM), X-ray photoelectron spectroscopy (XPS), Raman spectroscopy, and N_2 adsorption measurements. Photocatalytic rates of reaction are measured by following the degradation of cresol (UV−vis λ_{max} at 254 nm), a hole-dependent reaction,[25] and by following the photogeneration of hydroxyl radicals detected by measuring the intensity of 2-hydroxyterephthalic acid (which has a photoluminescence band at 425 nm formed by the reaction) between $OH^\bullet$ and terephthalic acid.[26]

Zinc gallate was synthesized hydrothermally from stoichiometric zinc, and gallium nitrate hydrates, at a pH set initially at 7.5 with concentrated ammonia.[27] Calcined product (0.25 g, heated to 873 K at 5 K/min, 5 h) was then stirred in an ethanolic solution. This suspension was added to a solution of tin chloride ($SnCl_2$ or $SnCl_4$, 80 or 160 mmol/L in 0.1 N HCl, the volume of HCl kept constant at 46 mL) maintained at 353 K and then stirred for 2 h (see Table 1). The resultant suspension was centrifuged, washed with DI water multiple times, and dried at 353 K to obtain the final product. The sample obtained with the $SnCl_2$ precursor was yellow, whereas that obtained with $SnCl_4$ was white. Yellow SnO_x powders were synthesized using $SnCl_2$ utilizing the same procedure described above but without adding zinc gallate particles to the synthesis solution. White rutile SnO_2 was prepared utilizing the same procedure but using $SnCl_4$ as the precursor. Detailed experimental procedures are in the Supporting Information.

XRD patterns (Figure 1A) show that the d[10] precursor obtained from hydrothermal synthesis is pure spinel $ZnGa_2O_4$. After the reaction of zinc gallate with tin precursors, irrespective of the tin source, new broad reflections (for example, at ~26.5° 2θ in Figure 1A) were observed. The absence of any peak shifts of XRD peak positions of zinc gallate rules out tin incorporation into the structure of $ZnGa_2O_4$. This is as expected because the ionic radius of Sn^{2+} is larger than that of Zn^{2+} and Ga^{3+}. These broad reflections were assigned to a SnO_2 (tetragonal) rutile nanophase (see Supporting Information). This result is not unexpected because the use of Sn(II) generally leads to partial oxidation, as confirmed using Mössbauer spectroscopy (Figure 2) of the SnZGO1 sample that has 79% Sn(IV) and 21% Sn(II).[13,28]

With the presence of this additional tin oxide phase, the intensity of the XRD reflections associated with $ZnGa_2O_4$ decreased. There is also a measurable increase in the fwhm for the (311) reflection with tin content and, therefore, a decrease in the effective particle size from 22 to 19 nm with 160 mmol of Sn (Table 1). Surface areas increase with tin incorporation from 55 m^2/g for the bare $ZnGa_2O_4$ oxide to 82 m^2/g for the SnZGO1 photocatalyst, possibly from the presence of SnO_x nanoparticles on the product zinc gallate. Figure 1B shows the high-resolution transmission electron microscopy (HR-TEM) image of the particles. The well-resolved lattice

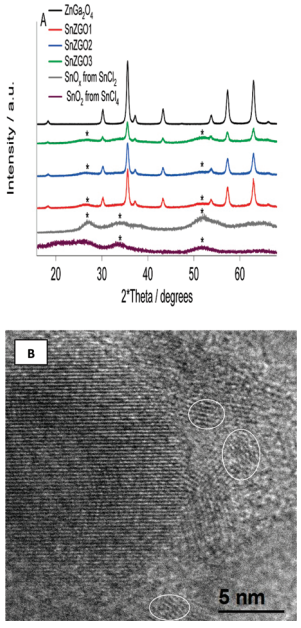

Figure 1. XRD patterns of Sn−ZGO materials. (A) The asterisk indicates the reflections associated with a rutile SnO_2 phase. The usage of a quartz sample holder for the SnO_2 from $SnCl_4$ sample precludes the initial peak of the rutile phase from being observed properly. The diffraction patterns of SnO_x and SnO_2 are magnified 6 times. (B) A representative HRTEM image of SnZGO1, which indicates zinc gallate decorated with small SnO_x nanoparticles, the latter in white ovals.

fringes of ~2.5 Å correspond to the (311) d spacing of zinc gallate having the spinel structure (JCPDS file no. 71-0843). Also noticeable in the image is that the larger $ZnGa_2O_4$ particle is decorated with smaller particles of SnO_x identified through the interplanar spacing (~3.3 Å) corresponding to the d spacing of the (110) plane of the rutile SnO_2 phase (JCPDS file no. 88-0287). The TEM image also indicates that the tin oxide particles are only 2−5 nm in dimensions, as would be expected from the broad peaks in the XRD patterns (Figure 1A).

Although the XRD patterns of the tin−$ZnGa_2O_4$ systems are similar, the UV−vis diffuse reflectance spectra are markedly different (Figure 3). When the tin precursor employed is a tin(II) source, the spectrum is red-shifted from 4.5 eV (276 nm) for $ZnGa_2O_4$ to 2.8 eV (443 nm) for the SnO_x−$ZnGa_2O_4$ materials. This absorbance edge in the visible region is associated with the presence of Sn^{2+} species. The presence of surface tin oxide species is also confirmed using XPS, which show higher tin concentrations on the surface than in the bulk. Mössbauer spectroscopy can be utilized to identify the oxidation state of tin.[28]

dx.doi.org/10.1021/cs200137h |ACS Catal. 2011, 1, 923–928

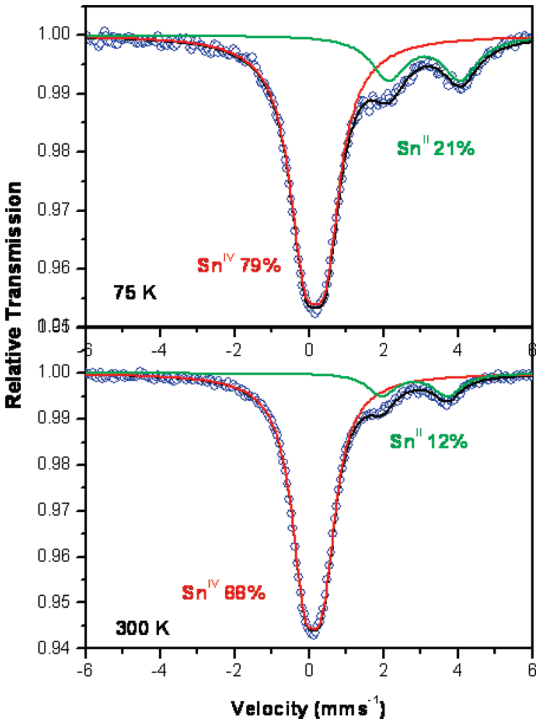

Figure 2. Mössbauer spectroscopy conducted at 75 and 300 K for SnZGO1 photocatalyst. The contribution of Sn(II) is higher from the Mössbauer spectrum obtained at 75 K than that measured at 300 K. Because at low temperatures, the differences between the values of the uncertainties for each species is minimized, the fraction of Sn(II) obtained from the low temperature analysis is more realistic.

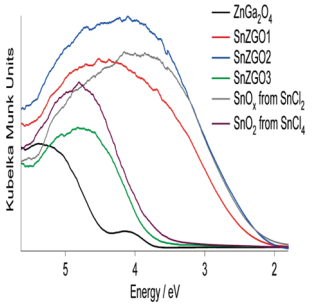

Figure 3. Diffuse reflectance spectra of Sn−ZGO materials. Also presented are that of zinc gallate and SnO_x nanoparticles.

The spectra analyzed at room temperature and at 75 K show that the tin in SnO_x phase exists in both the 2+ and 4+ oxidation states. The low temperature spectrum (Figure 2) indicates that the majority of tin from the $SnCl_2$ precursor has been oxidized to Sn(IV), but around 21% remains as Sn(II) (Table 2). Figure 2 then indicates that it is Sn(II) that contributes to a red shift in the absorbance spectra to the visible region (Figure 3) of the composite materials because when the synthesis was carried out using a $SnCl_4$, no significant decrease in the band gap was observed with the band gap measured at 3.9 eV, 318 nm (Table 1).

Similarly, when no tin source was employed, no decrease in the band gap of zinc gallate was observed. Furthermore, when the Sn^{2+} containing SnO_x−zinc gallate SnZGO1 material was calcined at 300 °C for 6 h, the absorbance edge blue-shifted to the UV region. The band gap in this case is 3.4 eV (see Supporting Information). This is due to an oxidation of Sn^{2+} to Sn^{4+}. A similar blue shift upon calcination has been noticed for Sn(II) compounds such as anatase Sn−TiO_2 and Sn−Nb−O pyrochlores.[28,29] These experiments confirm that the absorbance in the visible region of SnZGO1 and SnZGO2 composite materials is from the presence of Sn^{2+} species, although the exact location of Sn^{2+} in SnO_x still needs to be determined.

Table 2. Mössbauer ^{119}Sn Hyperfine Parameters of SnZGO1 Photocatalyst at 300 and 75 K[a]

analysis temp, K	isomer shift, δ mm/s	quadrupole splitting, Δ mm/s	line width, Γ mm/s	spectral weight %	site identification
300 K	0.022 (2)	0.483 (4)	0.87 (1)	88	Sn^{IV}
	2.74 (2)	1.77 (2)	0.89 (3)	12	Sn^{II}
75 K	0.062 (5)	0.567 (8)	1.00 (1)	79	Sn^{IV}
	3.01 (2)	1.94 (3)	1.13 (4)	21	Sn^{II}

[a] Isomer shifts are with respect to $BaSnO_3$.

The photocatalytic properties of the materials were assessed following the degradation of cresol using UV and visible (λ > 420 nm) light (Figure 4A). The photocatalysts with Sn(II) are reactive in visible light for the degradation of cresol. Irrespective of the fact that these materials are active in visible light, no decrease in UV light activity is observed upon the presence of the SnO_x species when compared with bare zinc gallate.[17,30] Many other photocatalysts are considerably less active using visible light than when using UV light because the introduced dopant orbitals are also localized recombination states either midgap (cation doped)[17] or above the VB (due to inhomogeneous anion doping).[25,30,31] The SnZGO2 sample especially shows only a small decrease in the rate of cresol oxidation using visible light (λ > 420 nm) compared with the rate of reaction observed using UV light (the full spectrum).

The oxidation of phenolic compounds proceeds via direct oxidation by holes.[25] This was corroborated by determining that there is no decrease in the effective rates of cresol oxidation with the addition of 2-propanol, a hydroxyl radical scavenger.[32] This implies that the effective photo-oxidative reactivity of holes increases after tin addition. The band structures of $ZnGa_2O_4$ (Yan et al.[33] and Zhang et al.[34]) and SnO_2 (Gratzel)[35] are in the references stated, though that for Sn^{2+} containing SnO_x material is yet to be determined. Recently, Oropoeza et al.[36] noticed a shift in the valence band edge toward the Fermi level using valence band and shallow core level photoemission spectroscopy techniques for Sn−TiO_2 systems. They have attributed this increase in the maximum of the valence band edge of titania to Sn(II) cations occupying surface and grain boundary sites. Nonetheless, further experimentation is required to clarify the electronic interactions between the surface SnO_x phase and zinc gallate.

The total amount of hydroxyl radicals determined by detecting the PL intensity of 2-hydroxyterephthalic acid[37] decreases when using only visible light compared with the use of UV light for SnZGO2 material (Figure 4B). This further corroborates that the degradation of cresol proceeds via direct oxidation by holes, because *no* substantive decrease in effective rates is observed when using visible light for the SnZGO2.[25] After 3 h of illumination, the amount of hydroxyl radicals in solution determined by the photoluminescence intensity of 2-hydroxyterephthalic acid (using SnZGO2 photocatalyst) is 6.8 (UV) and 2.1 (visible) times higher than the amount of hydroxyl radical species obtained when the bare zinc gallate photocatalyst is used in UV light. This improvement in the hydroxyl radical concentration suggests better

dx.doi.org/10.1021/cs200137h |*ACS Catal.* 2011, 1, 923–928

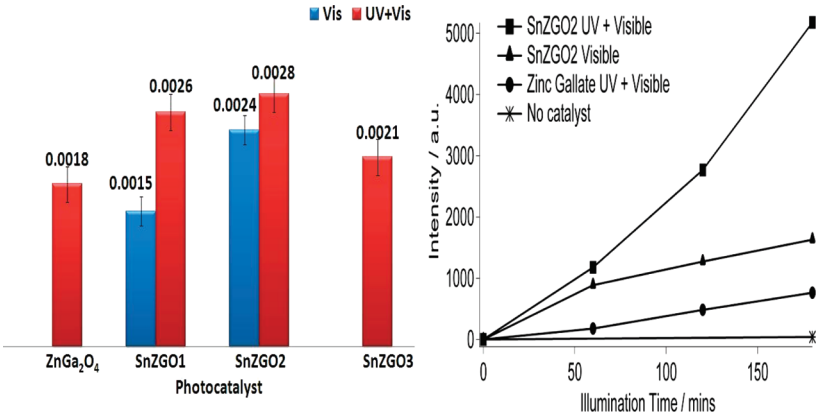

Figure 4. Effective rate constants (min^{-1}) of cresol degradation (A) and the concentration of hydroxyl radicals as measured by the PL intensity of 2-hydroxyterephthalic acid with the catalyst SnZGO2 (B) using UV (the full spectrum) and visible light (λ > 420 nm) conditions. The control experiments are in the Supporting Information.

charge separation for the SnO_x—$ZnGa_2O_4$ materials relative to zinc gallate. Control experiments were conducted (see the Supporting Information, Figure S2) with the catalyst in dark and without the catalyst in UV light. All show little conversion, demonstrating that the observed degradation of cresol is, indeed, photocatalytic. Furthermore, the SnO_x species individually (without zinc gallate) did not show any reactivity for cresol oxidation in visible light (only 5% degradation to quinone intermediates[25,38] was obtained after 4 h of illumination). We suggest that the design of other photocatalysts with higher effective photo-oxidative reactivity of holes may be possible by employing the simple hydrothermal surface modification procedure described here, thereby extending the range of visible-light-active materials.

Although the photocatalytic reactivity of these composite catalysts is clear, the surface structure/reconstruction upon the presence of the SnO_x species is not. $ZnGa_2O_4$ has five Raman-active modes —T_{2g}, E_g, T_{2g} (469 cm^{-1}), T_{2g} (611 cm^{-1}), A_{1g} (714 cm^{-1})— and one second-order mode at ~670 cm^{-1}. All these modes are associated with Zn—O tetrahedron vibrations.[8] With the additional surface tin phase, the bands associated with $ZnGa_2O_4$ decrease in intensity along with the appearance of a new broad band from 520 to 650 cm^{-1}, centered at ~580 cm^{-1}. This broad mode, interestingly, is not associated with the point group allowed modes of the additional SnO_2 phase detected in the XRD patterns (A_{1g} of SnO_2 is at 638 cm^{-1}). Dieguez et al.[39] observed a similar band, which they assigned to surface stresses induced from the presence of disordered surface tin oxide species. This observation suggests that there is a layer or a cluster of tin oxides on the surface of zinc gallate.[23] This is consistent with the XPS measurements wherein the surface tin contents are considerably higher (Table 1) than the bulk tin content in the solid (determined from energy dispersive X-ray spectroscopy at low magnifications).

Color-coded SEM elemental mapping was employed to verify for uniform distribution of the cations because the intensity and spread of the color is proportional to the corresponding element's concentration. This result (see Supporting Information) indicates that the distribution of tin over zinc gallate particles is uniform. The appearance of intense Raman bands for these disordered species compared with the weak bands for ordered $ZnGa_2O_4$ could be because the vibrational amplitudes of atoms and the electric fields generated by incident light of a surface species are larger than from the bulk constituents.[40] Thus, the

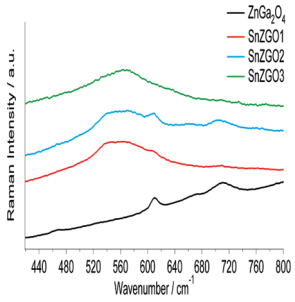

Figure 5. Raman spectra of Sn—ZGO materials. Also presented is that of zinc gallate.

Raman signal in Figure 5 is dominated by tin oxide surface species. This phenomenon has been noted for SnO_2 particles with surface disorder caused by a nonstoichiometric tin oxide surface layer by Dieguez et al.,[39] for core—shell type Si, Ge, and GaP particles by Hayashi and Yamamoto[40] and for Zn—ZnO core—shell materials by Zeng et al.[41] The Raman and XPS investigations therefore suggest the presence of nanoparticles on $ZnGa_2O_4$, as is also observed using HR-TEM (Figure 1B). Note that the additional peaks attributed to tin oxide species in the XRD patterns and Raman spectra for these SnZGO materials is in contrast to Sn(II)—TiO_2 materials developed earlier, wherein no such additional peaks were observed, suggesting the absence of an additional tin oxide phase for Sn(II)—TiO_2 photocatalysts.[42]

Because of the use of $SnCl_x$ precursors, there is also 1—3 wt % Cl in the materials (as determined from SEM—EDAX). This has been reported for Sn(IV)-doped titania materials synthesized using halide precursors,[43,44] but in those cases is not the major cause for the reduction in the band gap.[42] Chlorine, for instance, was also observed for the calcined SnZGO1 and SnZGO3 (from a $SnCl_4$ precursor) materials, yet their band gaps are in the UV region (3.4 and 3.9 eV, respectively). The chloride ion is then not the reason for the reduction in the band gaps of the SnZGO1 and SnZGO2 synthesized from $SnCl_2$ precursor. Note, however, that upon illumination, chlorine could form chloride radicals that can affect photocatalytic activity, as was noticed in our earlier study on Sn(II)—TiO_2 materials synthesized from $SnCl_2$ and $SnBr_2$ precursors[42]

dx.doi.org/10.1021/cs200137h |ACS Catal. 2011, 1, 923–928

To conclude, a d^{10} mixed-metal oxide photocatalyst was made responsive to visible light as a result of SnO_x surface species on zinc gallate, although work is still needed to better elucidate the structure of SnO_x and its electronic−structural interaction with zinc gallate. These photocatalysts are effective for the oxidation of cresol with rates, just in visible light (for SnZGO2 material), better than what is observed with the precursor zinc gallate using UV light. This result is probably associated with the unique structure of these materials, leading to an increased effective photo-oxidative reactivity of holes. This is a promising development because valence band holes can alone completely mineralize organic molecules and VOCs.[25,45] These materials also favor the generation of oxidizing hydroxyl radicals using visible light, suggesting their use for photocatalytic applications in which hydroxyl radical oxidation is desirable.

■ ASSOCIATED CONTENT

Supporting Information. Experimental details, application of Davis−Mott equation for calculation of band gaps, cresol degradation control experiments, PL curves of 2-hydroxyterephthalic acid with SnZGO2 catalyst, pore size distribution, color-coded SEM elemental mapping, additional XRD−diffuse reflectance spectra of calcined SnZGO1 and SnO_x materials, and SEM images of materials. This material is available free of charge via the Internet at http://pubs.acs.org.

■ AUTHOR INFORMATION

Corresponding Author

*Phone: 302-831-1261. Fax: 302-831-1048. E-mail: lobo@udel.edu.

■ ACKNOWLEDGMENT

The authors acknowledge F. Jiao for TEM images; N. Hould and K. Majnouka for help and suggestions during the course of the work; Dr. Jean-Claude Jumas at Université Montpellier II for Mössbauer spectroscopy; N. Menagazzo for help with the Raman scans; R. Opila, C. Weiland, and Fang Fang for training sessions on the XPS; A. Robinson and P. McNeely for time on the PL equipment; and C. Ni and F. Kriss of the W. M. Keck Electron Microscopy Facility at the U.D. for providing the scanning electron microscope time and help. Funding for this research was provided by the U.S. Department of Energy Basic Energy Sciences under Grants nos. DE-FG02-07ER15921 and DE-FG02-99ER14998.

■ REFERENCES

(1) National Academy of Engineering−Grand Challenges for Engineering; http://www.engineeringchallenges.org/.
(2) Hernandez-Alonso, M. D.; Fresno, F.; Suarez, S.; Coronado, J. M. *Energy Environ. Sci.* **2009**, *2*, 1231.
(3) Linsebigler, A.; Lu, G.; Yates, J. *Chem. Rev.* **1995**, *95*, 735.
(4) Maeda, K.; Teramura, K.; Lu, D.; Takata, T.; Saito, N.; Inoue, Y.; Domen, K. *Nature* **2006**, *440*, 295.
(5) Wang, X.; Maeda, K.; Lee, Y.; Domen, K. *Chem. Phys. Lett.* **2008**, *457*, 134.
(6) Inoue, Y. *Energy Environ. Sci.* **2009**, *2*, 364.
(7) Boppana, V. B. R.; Doren, D. J.; Lobo, R. F. *ChemSusChem* **2010**, *3*, 814.
(8) Ram Boppana, V. B.; Doren, D. J.; Lobo, R. F. *J. Mater. Chem.* **2010**, *20*, 9787.
(9) Yoshida, M.; Hirai, T.; Maeda, K.; Saito, N.; Kubota, J.; Kobayashi, H.; Inoue, Y.; Domen, K. *J. Phys. Chem. C* **2010**, *114*, 15510.
(10) Kudo, A.; Omori, K.; Kato, H. *J. Am. Chem. Soc.* **1999**, *121*, 11459.
(11) Oshikiri, M.; Boero, M.; Ye, J.; Zou, Z.; Kido, G. *J. Chem. Phys.* **2002**, *117*, 7313.
(12) Tang, J.; Zou, Z.; Ye, J. *Angew. Chem., Int. Ed.* **2004**, *43*, 4463.
(13) Hosogi, Y.; Shimodaira, Y.; Kato, H.; Kobayashi, H.; Kudo, A. *Chem. Mater.* **2008**, *20*, 1299.
(14) The effective photo-oxidative reactivity of holes is a combination of both oxidation potential of holes (which decreases with decreasing band gap when caused by VB hybridization) and the mobility of holes (this increases in a dispersed VB comprised of s orbitals). See: Liu, G.; Niu, P.; Wang, L.; Lu, G. Q.; Cheng, H.-M. *Catal. Sci. Technol.* **2011**, *1*, 222.
(15) Jin, Q.; Fujishima, M.; Tada, H. *J. Phys. Chem. C* **2011**, *115*, 6478.
(16) Tada, H.; Jin, Q.; Nishijima, H.; Yamamoto, H.; Fujishima, M.; S.-i. Okuoka, Hattori, T.; Sumida, Y.; Kobayashi, H.; , *Angew. Chem. Int. Ed.* **2011**, *50*, 3501.
(17) Nagaveni, K.; Hegde, M. S.; Madras, G. *J. Phys. Chem. B* **2004**, *108*, 20204.
(18) Davis, E. A.; Mott, N. F. *Philos. Mag.* **1970**, *22*, 903.
(19) Jiang, L.; Sun, G.; Zhou, Z.; Sun, S.; Wang, Q.; Yan, S.; Li, H.; Tian, J.; Guo, J.; Zhou, B.; Xin, Q. *J. Phys. Chem. B* **2005**, *109*, 8774.
(20) Firooz, A. A.; Mahjoub, A. R.; Khodadadi, A. A. *Mater. Lett.* **2008**, *62*, 1789.
(21) Zhu, J.; Lu, Z.; Aruna, S. T.; Aurbach, D.; Gedanken, A. *Chem. Mater.* **2000**, *12*, 2557.
(22) Kar, A.; Kundu, S.; Patra, A. *J. Phys. Chem. C* **2011**, *115*, 118.
(23) Liu, G.; Wang, L.; Yang, H. G.; Cheng, H.-M.; Lu, G. Q. *J. Mater. Chem.* **2010**, *20*, 831.
(24) Yu, H.; Irie, H.; Shimodaira, Y.; Hosogi, Y.; Kuroda, Y.; Miyauchi, M.; Hashimoto, K. *J. Phys. Chem. C* **2010**, *114*, 16481.
(25) Liu, G.; Niu, P.; Sun, C.; Smith, S. C.; Chen, Z.; Lu, G. Q.; Cheng, H.-M. *J. Am. Chem. Soc.* **2010**, *132*, 11642.
(26) Ishibashi, K.-i.; Fujishima, A.; Watanabe, T.; Hashimoto, K. *Electrochem. Commun.* **2000**, *2*, 207.
(27) Chen, X.; Xue, H.; Li, Z.; Wu, L.; Wang, X.; Fu, X. *J. Phys. Chem. C* **2008**, *112*, 20393.
(28) Ghosh, M.; Pralong, V.; Wattiaux, A.; Sleight, A.; Subramanian, M. *Chem.—Asian J.* **2009**, *4*, 881.
(29) Omata, T.; Kita, M.; Otsuka-Yao-Matsuo, S.; Katada, M. *J. Phys. Chem. Solids* **2005**, *66*, 53.
(30) Wang, J.; Tafen, D. N.; Lewis, J. P.; Hong, Z.; Manivannan, A.; Zhi, M.; Li, M.; Wu, N. *J. Am. Chem. Soc.* **2009**, *131*, 12290.
(31) Irie, H.; Watanabe, Y.; Hashimoto, K. *J. Phys. Chem. B* **2003**, *107*, 5483.
(32) Zhuang, J.; Dai, W.; Tian, Q.; Li, Z.; Xie, L.; Wang, J.; Liu, P.; Shi, X.; Wang, D. *Langmuir* **2010**, *26*, 9686.
(33) Yan, S. C.; Ouyang, S. X.; Gao, J.; Yang, M.; Feng, J. Y.; Fan, X. X.; Wan, L. J.; Li, Z. S.; Ye, J. H.; Zhou, Y.; Zou, Z. G. *Angew. Chem., Int. Ed.* **2010**, *49*, 6400.
(34) Zhang, W.; Zhang, J.; Lan, X.; Chen, Z.; Wang, T. *Catal. Commun.* **2010**, *11*, 1104.
(35) Gratzel, M. *Nature* **2001**, *414*, 338.
(36) Oropeza, F. E.; Davies, B.; Palgrave, R. G.; Egdell, R. G. *Phys. Chem. Chem. Phys.* **2011**, *13*, 7882.
(37) Liu, G.; Wang, L.; Sun, C.; Yan, X.; Wang, X.; Chen, Z.; Smith, S. C.; Cheng, H.-M.; Lu, G. Q. *Chem. Mater.* **2009**, *21*, 1266.
(38) Andersson, M.; Österlund, L.; Ljungström, S.; Palmqvist, A. *J. Phys. Chem. B* **2002**, *106*, 10674.
(39) Dieguez, A.; Romano-Rodriguez, A.; Vila, A.; Morante, J. R. *J. Appl. Phys.* **2001**, *90*, 1550.
(40) Hayashi, S.; Yamamoto, K. *Superlattices Microstruct.* **1986**, *2*, 581.
(41) Zeng, H.; Cai, W.; Cao, B.; Hu, J.; Li, Y.; Liu, P. *Appl. Phys. Lett.* **2006**, *88*, 181905.

(42) Boppana, V. B. R.; Lobo, R. F. *J. Catal.* **2011**; doi: 10.1016/j.jcat.2011.04.014.
(43) Li, J.; Zeng, H. C. *J. Am. Chem. Soc.* **2007**, *129*, 15839.
(44) Yu, J.; Liu, S.; Zhou, M. *J. Phys. Chem. C* **2008**, *112*, 2050.
(45) Qiu, X.; Miyauchi, M.; Yu, H.; Irie, H.; Hashimoto, K. *J. Am. Chem. Soc.* **2010**, *132*, 15259.